

Pulsar Navigation

Josep Sala, Andreu Urruela, Xavier Villares, Jordi Romeu, Sebastià Blanch
Dpt. of Signal Theory and Communications, Technical University of Catalonia (UPC)
c/Jordi Girona 1-3, Campus Nord UPC, D5-114b, 08034 Barcelona, SPAIN
Phone:+34-93-4015894, Fax:+34-93-4016447, E-mail: josep.sala@upc.edu

Robert Estalella, Josep M. Paredes
Dpt. of Astronomy and Meteorology, University of Barcelona (UB)
Diagonal 647, E-08028 Barcelona, SPAIN
E-mail: robert@am.ub.es,jmparedes@ub.edu *

January 14, 2008

Abstract

This paper evaluates the fundamental performance bounds, signal processing and technological complexity associated with the synchronization to radio and X-ray pulsars as well as its impact on the positioning accuracy of an autonomous spacecraft navigation system. Performance analysis of synchronization and location algorithms builds on Maximum Likelihood (ML) estimation which provides, asymptotically, unbiased minimum variance estimates with mean square error strictly approaching the Cramer-Rao Lower Bound (CRLB).

1 Introduction

Pulsar grids have been suggested in the past for autonomous, earth-independent, deep space location and for the establishment of a universal time base. This paper summarizes a feasibility study of deep space navigation based

on radio and X-ray pulsar timing information. The analysis is focused on the signal processing aspects of the system according to the structure in figure (1). Therefore, the quality of measurements attainable with on-board instrumentation is evaluated for realistic space scenarios for the selected pulsars.

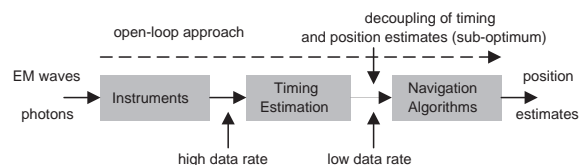


Figure 1: Navigation system structure. The first stage (instruments) converts EM waves/photons to raw digital input signals. Decoupling of timing (second stage) and location (third stage) parameter estimation is considered for ease of implementation and obtention of closed-form expressions of performance measures. Timing estimation uses information from a pulsar database to compare measured with expected pulse arrival times. The location stage uses this differential information to derive a position estimate.

*European Space Agency (ESA), project ARIADNA 03/4202 "Feasibility Study of a Spacecraft Navigation System relying on Pulsar Timing Information" April-June 2004.

Radio pulsars [1] are broadband stellar pulsating radio sources powered by the rotation of a neutron star, implying a great stability of the pulsar period (in the millisecond to second range), which steadily increases as the pulsar releases its rotational energy. Some 1300 pulsars are known [2], and more are discovered in every new survey [3]. Most of millisecond pulsars belong to binary systems, their pulse arrival time affected by the system orbital motion. In some pulsars, irregularities (glitches) in their rotation speed ω have been observed every few years, with fractional changes in the order of 10^{-6} for the Vela pulsar, while only 10^{-8} for the Crab pulsar. Pulsars emit a pulse of radiation during a small fraction of the rotation period. Although individual pulses vary in strength and shape (micro-structure), the average pulse shape is stable and characteristic of each pulsar. Very precise models have been established for the mean arrival time of pulsars whose extraordinary stability outperforms the most precise artificial time-bases. The most stable are millisecond pulsars. Unfortunately, their SNR is considerably poorer than for other longer period pulsars. Radio pulsars have steep power-law spectra, with spectral indices α ($S_\nu \propto \nu^\alpha$) ranging from -3.0 to -0.1 , with a median of ~ -1.7 . The strongest pulsar at 1 GHz has a flux density of 1.7 Jy (1 Jansky = 10^{-26} W m $^{-2}$ Hz $^{-1}$).

X-ray pulsars can be grouped in two different families according to the powering source: accretion- and rotation-powered pulsars. Accretion-powered pulsars are found in X-ray binary systems, the brightest class of X-ray sources in the sky. An X-ray binary contains either a neutron star or a black hole accreting material from a companion star. A neutron star with a strong magnetic field ($\sim 10^{12}$ G) will disrupt the accretion flow at several hundred neutron star radii and funnel material onto the magnetic poles. If the magnetic and rotation axes are misaligned, X-ray pulsations

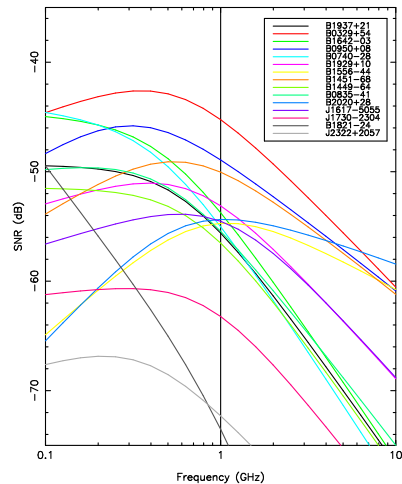


Figure 2: SNR as a function of frequency for the observation of the 15 best Q pulsars, assuming an effective area $A_e = 10$ m 2 , a beam efficiency $\eta_M = 0.9$, and no contribution from the Sun emission.

will be observed if the beamed emission from the magnetic poles rotates through the line of sight. Thirty-two accretion-powered X-ray pulsars have been discovered [4], with pulse periods distributed between 0.069 s and 835 s. Long term monitoring has revealed different types of behaviour for the pulse period: a) linear decrease with time (spin-up) with erratic variations around the trend, b) no long term trend and only a random walk in the period, c) a steady increase in the period (spin-down). The pulse period fluctuations reflect inhomogeneities in the accretion flow, which excludes these pulsars as a stable timing source. Rotation-powered pulsars are rapidly spinning, strongly magnetized neutron stars radiating at the expense of rotational energy. For a long time the most luminous of all rotation-powered pulsars, the Crab pulsar, had been the only radio pulsar detected at X-ray energies. Today, as a result of observations with ROSAT and ASCA,

27 pulsars have been detected [5], with a range of spin periods between 1.6 ms and 530 ms. However, some of them have shown lack of pulsed emission at X-rays and/or the presence of glitches. This excluded them from our list of suitable candidates. Ten X-ray pulsars were finally selected [6]. Millisecond pulsars are distinguished by their small spin periods ($P \leq 20$ ms) and high rotational stability ($dP/dt \simeq 10^{-18} - 10^{-21}$). Among the selected rotation-powered pulsars with pulsed X-ray emission, there are four millisecond pulsars (PSR J0437-47, PSR B1821-24, PSR J2124-33 and PSR J0030+0451). PSR J0030+0451 was recently discovered, presenting a period of 4.8 ms and gross similarity between the radio and the X-ray pulse profile (Becker et al. 2001). In the case of PSR B1821-24, the pulse profile has narrow peaks while for PSR J0437-47 and PSR J2124-33 the pulse profiles are broad.

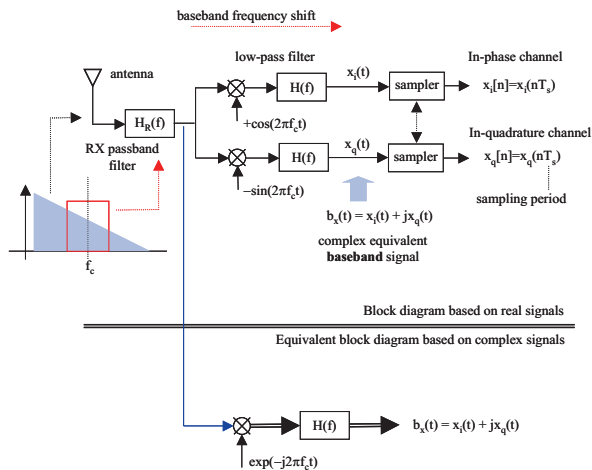


Figure 3: (Above) Signal processing scheme (IQ-sampling) for generating the in-phase and in-quadrature components of a passband radio signal at the central frequency f_c . (Below) Equivalent representation in complex notation.

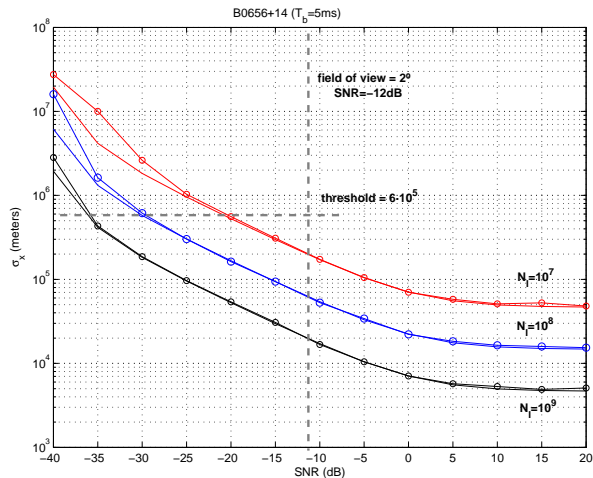


Figure 4: Standard deviation of the range estimator (in meters) for the B0656+14 X-Ray pulsar as a function of the SNR. Different integration times are considered and both the ML estimator (round markers) and the related CRB bound (no markers) are depicted. The low-SNR threshold is also shown in the figure.

2 Current Research

In this section we describe accomplished research on: (a) the fundamentals of radio- and X-ray pulsar synchronization, which, according to the structure in figure (1), is the previous step to navigation algorithms; (b) a simple navigation algorithm suitable for feasibility analysis, which incorporates ambiguity resolution. Conclusions and future vision will be provided in forthcoming sections.

2.1 Radio Pulsar Synchronization

Due to pulsar rotation, the noiseless pulsar signal $x_p(t)$ is described as a random signal with periodically time-varying statistics. That is, $x_p(t)$ is a cyclo-stationary stochastic process [7], with auto-correlation function $r_{x_p x_p}(t, \tau) = \mathbb{E}[x_p^*(t)x_p(t + \tau)]$ depending on the delay variable τ and periodic in the time variable t , with

$\mathbb{E}[\cdot]$ the expectation operator. We denote the inverse of this rotation frequency the Pulse Repetition Period (PRP) T . Then, the k -th period of $x_p(t)$, corresponding to the time interval $[-T/2+kT, T/2+kT)$, displays a broadband micro-structure constituted by a number of random sub-pulses. The instantaneous power profile of $x_p(t)$ is defined as,

$$\sigma_p^2(t) = r_{x_px_p}(t; 0) = \mathbb{E}|x_p(t)|^2 \quad (1)$$

After propagating through the interstellar medium, $x_p(t)$ experiences a frequency dependent time delay $T(f) = T_\infty - D(r)f^{-2}$ that distorts the broadband pulse envelope, with the dispersion parameter $D(r)$ depending on the distance r from the pulsar. As $x_p(t)$ extends over many octaves, multi-channel processing for pulsar observation is usually carried out over a fraction of its broadband spectrum. Considering a single channel, a portion of that spectrum is pass-band filtered at the central frequency of the antenna: $x_h(t) = h_R(t) * x_p(t)$ (with $*$ the convolution operator and $h_R(t)$ the front-end filter impulse response), converted to base-band from the channel central frequency f_C and low-pass filtered by the analysis filter impulse response $h_b(t)$,

$$b(t) = h_b(t) * (e^{-j2\pi f_C t} \cdot x_h(t)) \quad (2)$$

to deliver the complex equivalent baseband signal $b(t)$, as shown in figure (3). Consecutive samples of $b(t)$, $b[n] = b(nT_s)$, with T_s the sampling period, are stored in vector \mathbf{x} . In fact, the pulsar signal $x_h(t)$ is immersed in radio noise from the Sun and the Galaxy, so that incorporating the equivalent baseband noise into \mathbf{x} , we get $\mathbf{x} = \mathbf{p}_\theta + \mathbf{n}$, with \mathbf{p}_θ and \mathbf{n} vectors of samples of the pulsar and noise processes, respectively; $\underline{\theta} = [\tau]$ constitutes the vector of unknown pulsar parameters, with τ the arrival phase of the pulsar signal with respect to the local timing reference. Although a more elaborate model might consider $\underline{\theta} = [\tau; \delta_\tau]$, where

the extra parameter δ_τ models pulsar period errors (frequency errors) in the local timing reference, meaningful feasibility results can already be obtained from this simplified model.

Pulsar phase synchronization constitutes the first stage in the navigation algorithms. In establishing the performance of pulsar synchronization, we assume the low-SNR Maximum Likelihood (ML) Estimator under complete knowledge of the pulsar and noise statistics, which is, asymptotically, a minimum variance unbiased estimator [8]. This estimator maximizes the probability density of the received signal conditioned on the unknown parameters (pulsar arrival phase): $p(\mathbf{x}|\tau)$. At low SNR (small antenna), its performance is controlled solely by the second order statistics (correlation matrix) of the pulsar signal, which can be (partially) inferred from experimental results. Hence, the pulsar instantaneous power profile $\sigma_p^2(t)$ is used as the only available information. Therefore, under Gaussian noise, the final phase estimate is found to be,

$$\hat{\tau} = \underset{\tau}{\operatorname{argmax}} (\mathbf{x}^H \mathbf{R}_n^{-1} \mathbf{R}_p(\tau) \mathbf{R}_n^{-1} \mathbf{x}) \quad (3)$$

where \mathbf{x} is a vector containing contiguous samples of the baseband received signal, \mathbf{R}_n is the correlation matrix of noise and $\mathbf{R}_p(\tau)$ is a model for the correlation matrix of the pulsar signal depending on the unknown phase parameter τ , which contains $\sigma_p^2(t)$ in its diagonal. This equation is applicable whatever the structure of \mathbf{R}_n and $\mathbf{R}_p(\tau)$, which makes it suitable for the multiband case. The phase estimator becomes the maximization of $J(\tau)$, where,

$$J(\tau) = \sum_{i=-N_1}^{+N_1} \operatorname{SNR}_i \cdot \sum_n |x_i[n]|^2 \sigma_b^2(\tau - \phi_i + nT_s)$$

with SNR_i the signal to noise ratio in the i -th subband, $N_{\text{sb}} = 2N_1 + 1$ the number of subbands, $x_i[n]$ the sampled signal in each subband and ϕ_i the pulsar phase delay due to interstellar dispersion in each subband.

The Cramer-Rao Lower Bound (CRLB) is a lower bound to the variance of the unbiased estimate of a parameter [8]. As the size of the data record grows to infinity, the CRLB constitutes a strict performance measure of the (asymptotically unbiased) ML estimator. For an unbiased estimate $\hat{\tau}_{\mathbf{x}}$ of τ , we have,

$$\text{CRLB}(\tau) = \mathbb{E}_{\mathbf{x}}|\hat{\tau}_{\mathbf{x}} - \tau|^2 \geq \frac{-1}{E_{\mathbf{x}}\nabla_{\tau}^2 \ln p(\mathbf{x}|\tau)}$$

in terms of the conditional data probability density $p(\mathbf{x}|\tau)$ evaluated at the true parameter τ . For a multiband processor the CRLB of the pulsar phase can be found expressed by the following equality,

$$\text{CRLB}_{\text{mb}}(\tau) = \frac{1}{4\pi^2 T_o B} \left(\frac{\sigma_n^2}{\sigma_{p,T}^2} \right)^2 \cdot \gamma_p^2 \cdot \xi_p^2 \quad (4)$$

with T_o the observation time, B the global bandwidth, σ_n^2 the noise power, $\sigma_{p,T}^2$ the pulsar average power (over the pulsar period) and γ_p^2 and ξ_p^2 two power-independent factors which depend on the shape of the power profile and power spectral density of the pulsar, respectively. The spectral shape factors ξ_p^2 is described by the following equation,

$$\xi_p^2 = \frac{\sigma_{p,T}^4}{\sigma_n^4} \left(\frac{1}{N_{\text{sb}}} \sum_{i=1}^{N_{\text{sb}}} \text{SNR}_i^2 \right)^{-1} \quad (5)$$

with SNR_i the signal to noise ratio in the i -th subband. The temporal shape factor γ_p^2 is given by,

$$\gamma_p^2 = \frac{N_T^2 \sigma_{p,T}^4}{\sum_{i=0}^{N_T-1} |(d\sigma_p^2/d\tau)(iT_s)|^2} \quad (6)$$

which is sensitive to the derivative of the pulsar power profile $\sigma_p^2(t)$: 'peaky' profiles are good for synchronization.

In the previous derivation, the pulsar frequency relative to the spacecraft frame of reference has been assumed known. A more complete study incorporates the estimation of the

pulsar frequency. Nevertheless, under a constant speed model, the CRLB of the pulsar phase coincides with the previously derived equation. Moreover, the pulsar phase estimation errors are statistically independent from the pulsar frequency estimation errors and the phase estimation corresponds to the phase in the middle of the integration period.

2.2 X-ray Pulsar Synchronization

The output of an X-ray detector can be modeled as a Poisson point process, with each event a photon arrival. A *stationary* Poisson point process is characterized by its mean event density (ideally, each event has zero duration) as $\lambda = \lim_{T_o \rightarrow \infty} (n(T_o)/T_o)$ with T_o the observation time and $n(T_o)$ the number of events in T_o . X-ray pulsars are characterized by a *cyclo-stationary* (periodic) probability density of emission. The addition of two independent Poisson point processes (X-Ray pulsar single photon arrival and Galaxy X-Ray Background) has an equivalent arrival density $\lambda(t) = \lambda_p(t) + \lambda_n$, with $\lambda_p(t) \ll \lambda_n$ the periodic pulsar arrival density and λ_n the stationary background contribution. The time resolution of the X-Ray detector is such that if more than one photon arrives within a given time-bin, it is detected as a single photon. For $\lambda(t) \simeq \lambda$ within a given time bin, the probability that k Poisson points occur in an interval of time T_b is provided by the relationship,

$$\text{Pr}(k) = \frac{(\lambda T_b)^k}{k!} \cdot e^{-\lambda T_b}$$

Hence, we have to distinguish two cases: (a) no photon has arrived in a given time-bin of duration T_b ; (b) more than one photon has arrived in the given time-bin. Their respective probabilities are,

$$P_0 = e^{-\lambda T_b} \quad , \quad P_1 = 1 - e^{-\lambda T_b} \quad (7)$$

Detection is modeled by an indicator function I_{n_1, n_2} that asserts whether events are detected

in the time bin $t_{n_1, n_2} = n_1T + n_2T_b = (n_1N_b + n_2)T_b$, with N_b the number of bins per period and T_b the detector time resolution. Then, P_0 and P_1 in (7) are expressed from,

$$\begin{aligned} P_0(n_2T_b) &= \Pr\{I_{n_1, n_2} = 0\} = e^{-\lambda(n_2T_b)T_b} \\ P_1(n_2T_b) &= \Pr\{I_{n_1, n_2} = 1\} = 1 - P_0(n_2T_b) \end{aligned}$$

From the above signal model, the ML criterion consists in maximizing the log-likelihood function $\ln p_I(I|\tau)$ with respect to the pulsar phase τ . Establishing the following probability estimate,

$$\hat{P}_1(n_2) = \frac{1}{N_I} \sum_{n_1=0}^{N_I-1} I_{n_1, n_2} \quad (8)$$

with $\hat{P}_0(n_2) = 1 - \hat{P}_1(n_2)$, the phase estimate is obtained as the maximization of $J(\tau)$,

$$J(\tau) = C_1 + N_I \sum_{n_2=0}^{N_b-1} \hat{P}_1(n_2) P(n_2T_b - \tau) \quad (9)$$

where $C_1 = -N_I T_b \sum_{n_2=0}^{N_b-1} \lambda(n_2T_b - \tau)$ is independent of τ provided that the bandwidth of $\lambda_p(t)$ is less than $0.5/T_b$ and, $P(t)$ is defined as

$$P(t) = \ln \left(e^{T_b \lambda(t)} - 1 \right) \quad (10)$$

The CRLB corresponding to this approximate ML formulation results in,

$$\begin{aligned} \text{CRLB}_{\text{low}}^{-1}(\tau) &= \frac{N_I T_b^2}{e^{T_b \lambda_n} - 1} \sum_{n_2=0}^{N_b-1} \lambda_p'^2(n_2T_b) \\ &\simeq \frac{N_I T_b}{e^{T_b \lambda_n} - 1} \int_0^T \lambda_p'^2(t) dt \leq N_I \lambda_n^{-1} \int_0^T \lambda_p'^2(t) dt \end{aligned} \quad (11)$$

with T_b the duration of the X-ray detector's time bin, N_b the number of bins per pulsar period, N_I the number of integrated pulsar periods and $\lambda_p'(t) = d\lambda_p(t)/dt$.

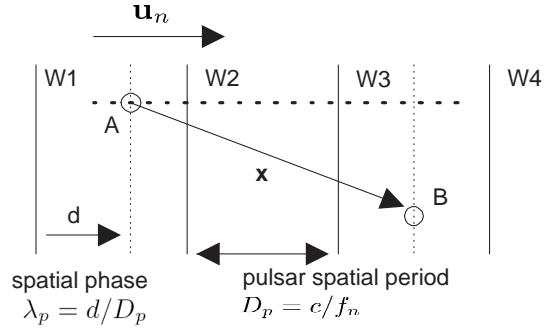


Figure 5: Geometrical interpretation of the phase estimate corresponding to time $t = T'_0 + (t - T'_0)$ as a snapshot depicting the pulsar wavefronts (W) as reference. The correction with respect to the reference position (Solar System Barycenter: point A) is represented by \mathbf{x} . The source of ambiguity is observed as an integer number of spatial pulsar periods D_p in the direction \mathbf{u}_n of the pulsar.

2.3 Pulsar Based Navigation

The extreme frequency stability of pulsars allows to predict the phase evolution of the pulsar signal in terms of barycentric time anywhere in the solar system using: (a) a previous estimate of the phase evolution for a reference time T_0 , (b) an estimate of the pulse frequency and (c) its multiple derivatives. The normalized barycentric phase evolution can be expressed as follows,

$$\begin{aligned} \Phi_k^{\text{SSB}}(t_o) &= [\Phi_k^{\text{SSB}}(T_0) + f_k \cdot (t_o - T_0) + \\ &+ \sum_{m=2}^M \frac{f_k^{(m)} \cdot (t_o - T_0)^m}{m!}]_w \end{aligned} \quad (12)$$

with t_o the current unknown time when phase is observed, $\Phi_k^{\text{SSB}}(t_o)$ the phase of the k -th pulsar at t_o , $f_k = 1/T_k$ the known frequency of the k -th pulsar, with T_k its period, $f_k^{(m)}$ its m -th known derivative and $[\cdot]_w$ the phase wrapping operation defined as,

$$0 \leq [\Phi]_w = \Phi + m_\Phi < 1 \quad (13)$$

with m_Φ the integer satisfying the previous condition. For t_o close to the time reference T_0 , we can consider only the first term in the Taylor series (12). Hence, at position \mathbf{x} w.r.t the SSB, phase observations become,

$$\begin{aligned}\widehat{\Phi}_n^{\mathbf{x}}(t_o) &= [\Phi_k^{\text{SSB}}(t_o - \tau_k) + w_{\Phi_k}]_w \quad (14) \\ &= [\Phi_k^{\text{SSB}}(T_0) + f_k \cdot (t_o - \tau_k - T_0) + w_{\Phi_k}]_w\end{aligned}$$

with $\widehat{\Phi}_n^{\mathbf{x}}(t_o)$ the phase observation associated with the k -th pulsar at time t_o (the superindex \mathbf{x} is used to denote a spacecraft measurement), τ_k the phase delay w.r.t the SSB and w_{Φ_k} an additive Gaussian noise term associated with the estimation of $\widehat{\Phi}_n^{\mathbf{x}}(t)$. The delay τ_k w.r.t. the SSB depends linearly on the spacecraft position \mathbf{x} as depicted in figure (5): $\tau_k = \frac{\mathbf{u}_k^T \mathbf{x}}{c}$, with \mathbf{u}_k a unitary vector from the SSB to the pulsar (note that \mathbf{u}_k does not depend on \mathbf{x}). Using this definition of τ_k in (15), $\widehat{\Phi}_n^{\mathbf{x}}(t_o) =$

$$\left[\Phi_k^{\text{SSB}}(T_0) + f_k \cdot \left(\Delta t_o - \frac{\mathbf{u}_k^T \mathbf{x}}{c} \right) + w_{\Phi_k} \right]_w$$

with $\Delta t_o = t_o - T_0$. Applying the wrapping operation in (13), $\lambda_k = \widehat{\Phi}_n^{\mathbf{x}}(t) - \Phi_k^{\text{SSB}}(T_0) =$

$$f_k \Delta t_o - \frac{f_k \mathbf{u}_k^T \mathbf{x}}{c} + m_k + w_{\Phi_k} \quad (15)$$

with λ_k the modified phase observation and m_k the unknown number of phase-cycles associated with the k -th pulsar. In vector notation,

$$\boldsymbol{\lambda} = \mathbf{U} \tilde{\mathbf{x}} + \mathbf{m} + \mathbf{w}_\lambda \quad (16)$$

where the following column vectors are defined,

$$\begin{aligned}\boldsymbol{\lambda} &= [\lambda_1; \dots; \lambda_K] \\ \tilde{\mathbf{x}} &= [\mathbf{x}; \Delta t_o] \\ \mathbf{m} &= [m_1; \dots; m_K] \\ \mathbf{w}_\lambda &= [w_{\Phi_1}; \dots; w_{\Phi_K}]\end{aligned}$$

and \mathbf{U} is defined as a $K \times (3 + 1)$ matrix,

$$\mathbf{U} = [\mathbf{U}_0, \mathbf{f}] = \begin{bmatrix} -\frac{f_1}{c} \mathbf{u}_1^T & f_1 \\ \vdots & \vdots \\ -\frac{f_K}{c} \mathbf{u}_K^T & f_K \end{bmatrix} \quad (17)$$

with \mathbf{f} the last column of \mathbf{U} , associated with the time variable. Note in (16) that the observation vector $\boldsymbol{\lambda}$ depends linearly on the unknown parameters $\tilde{\mathbf{x}}$ but is corrupted by an unknown integer vector \mathbf{m} . The determination of \mathbf{m} constitutes the ambiguity problem and it is a detection rather than an estimation problem.

2.3.1 ML Ambiguity Resolution

In the signal model shown in (16), we have two unknowns: the spacecraft's position and time estimate $\tilde{\mathbf{x}}$ and the unknown integer vector \mathbf{m} . The estimation of \mathbf{m} is the most difficult part since its support is the integer numbers. We define $\mathbb{M}[\mathbf{v}, \mathbf{M}] = \mathbf{v}^H \mathbf{M} \mathbf{v}$ for a dummy vector \mathbf{v} , with \mathbf{M} a non-negative definite matrix. Then, ambiguity resolution becomes,

$$\left(\widehat{\tilde{\mathbf{x}}}, \widehat{\mathbf{m}} \right) = \arg \min_{\tilde{\mathbf{x}}, \mathbf{m} \in \mathbb{Z}^K} [\mathbb{M}(\boldsymbol{\lambda} - \mathbf{m} - \mathbf{U} \tilde{\mathbf{x}}, \mathbf{R}_\lambda^{-1})] \quad (18)$$

where it is assumed that $\mathbf{w}_\lambda \sim \mathcal{N}(\mathbf{0}, \mathbf{R}_\lambda)$ (Gaussian distributed with mean $\mathbf{0}$ and correlation matrix \mathbf{R}_λ). We adopt here the Conditional ML approach (CML) where we calculate an estimate of $\tilde{\mathbf{x}}$ dependent on a dummy \mathbf{m} ,

$$\begin{aligned}\widehat{\tilde{\mathbf{x}}}(\mathbf{m}) &= \arg \min_{\tilde{\mathbf{x}}} [\mathbb{M}(\boldsymbol{\lambda} - \mathbf{m} - \mathbf{U} \tilde{\mathbf{x}}, \mathbf{R}_\lambda^{-1})] \\ &= (\mathbf{U}^T \mathbf{R}_\lambda^{-1} \mathbf{U})^{-1} \mathbf{U}^T \mathbf{R}_\lambda^{-1} \cdot (\boldsymbol{\lambda} - \mathbf{m}) \\ &= \mathbf{U}^\# (\boldsymbol{\lambda} - \mathbf{m})\end{aligned} \quad (19)$$

with $\mathbf{U}^\#$ implicitly defined. This estimate is plugged back into (18) to derive an estimate for \mathbf{m} as,

$$\widehat{\mathbf{m}} = \arg \min_{\mathbf{m} \in \mathbb{Z}^K} [\mathbb{M}(\boldsymbol{\lambda} - \mathbf{m} - \mathbf{U} \widehat{\tilde{\mathbf{x}}}(\mathbf{m}), \mathbf{R}_\lambda^{-1})]$$

This constitutes an integer weighted least squares problem over an infinite integer lattice with cost function $\psi_1(\mathbf{m}) =$

$$\begin{aligned}&= \mathbb{M}(\boldsymbol{\lambda} - \mathbf{m} - \mathbf{U} \widehat{\tilde{\mathbf{x}}}(\mathbf{m}), \mathbf{R}_\lambda^{-1}) \quad (20) \\ &= (\boldsymbol{\lambda} - \mathbf{m})^T \mathbf{R}_\lambda^{-1} (\mathbf{I} - \mathbf{U} \mathbf{U}^\#) (\boldsymbol{\lambda} - \mathbf{m})\end{aligned}$$

The hereto described technique for ambiguity resolution constitutes a cold-start scheme with no a priori information on the aircraft's position, where $\psi_1(\mathbf{m})$ requires minimization over a wide region of the multi-dimensional integer grid $\mathbf{m} \in \mathbb{Z}^K$. Note though, that as $\mathbf{M} = \mathbf{R}_\lambda^{-1}(\mathbf{I} - \mathbf{U}\mathbf{U}^\#)$ is rank-deficient, there may exist a wide (possibly infinite) range of values for \mathbf{m} almost parallel to the null subspace of \mathbf{M} , which yield a very low (and therefore likely) value of $\psi_1(\mathbf{m})$. Moreover, each of these solutions may correspond to very far locations which are difficult to discriminate (similar values of $\psi_1(\mathbf{m})$) and might easily give rise to an ambiguity resolution error. This problem is addressed in the following section with the incorporation of side information from previous estimations.

2.3.2 Bayesian Ambiguity Resolution

We model the observation vector $\boldsymbol{\lambda}$ (introduced in (16)) and the a priori information about $\tilde{\mathbf{x}}$ as Gaussian random variables,

$$\begin{aligned}\boldsymbol{\lambda} &\sim \mathcal{N}(\mathbf{U}\tilde{\mathbf{x}} + \mathbf{m}, \mathbf{R}_\lambda) \\ \tilde{\mathbf{x}} &\sim \mathcal{N}(\tilde{\mathbf{x}}_o, \mathbf{C}_{\tilde{\mathbf{x}}_o})\end{aligned}\quad (21)$$

Now, after some mathematical operations, we can obtain the unconditioned PDF of $\boldsymbol{\lambda}$ as,

$$\begin{aligned}p(\boldsymbol{\lambda}) &= \int p(\boldsymbol{\lambda}|\tilde{\mathbf{x}})p(\tilde{\mathbf{x}})d\tilde{\mathbf{x}} \\ &= p_0 \cdot e^{-\frac{1}{2}\mathbb{M}(\boldsymbol{\lambda} - \mathbf{m} - \mathbf{U}\tilde{\mathbf{x}}_o, [\mathbf{R}_\lambda + \mathbf{U}\mathbf{C}_{\tilde{\mathbf{x}}_o}\mathbf{U}^T]^{-1})}\end{aligned}\quad (22)$$

The Bayesian estimate of \mathbf{m} becomes $\hat{\mathbf{m}}_B = \arg \max_{\mathbf{m} \in \mathbb{Z}^K} p(\boldsymbol{\lambda}) =$

$$\arg \min_{\mathbf{m} \in \mathbb{Z}^K} \mathbb{M}(\boldsymbol{\lambda} - \mathbf{m} - \mathbf{U}\tilde{\mathbf{x}}_o, [\mathbf{R}_\lambda + \mathbf{U}\mathbf{C}_{\tilde{\mathbf{x}}_o}\mathbf{U}^T]^{-1})\quad (23)$$

Although this new cost function is different from $\psi_1(\mathbf{m})$, it can be proved that,

$$\hat{\mathbf{m}}_B = \arg \min_{\mathbf{m} \in \mathbb{Z}^K} (\psi_1(\mathbf{m}) + \psi_2(\mathbf{m}))\quad (24)$$

where $\psi_1(\mathbf{m})$ is defined in (20) and the new term $\psi_2(\mathbf{m})$ is defined as $\psi_2(\mathbf{m}) =$

$$= \mathbb{M}\left(\hat{\tilde{\mathbf{x}}}(\mathbf{m}) - \tilde{\mathbf{x}}_o, \left(\mathbf{C}_{\tilde{\mathbf{x}}_o} + (\mathbf{U}^T \mathbf{R}_\lambda^{-1} \mathbf{U})^{-1}\right)^{-1}\right)\quad (25)$$

with $\hat{\tilde{\mathbf{x}}}(\mathbf{m})$ defined in (19). We observe that a priori information has been expressed as the correction term $\psi_2(\mathbf{m})$ to the original cost function, which limits the integer search for \mathbf{m} .

For reasons of space, we have not included the covariance matrix of the position and time errors, which depends on the angular position of the pulsars. Rather we will be using the equivalent error obtained from c (speed of light) times the timing error.

3 Conclusions

As far as signal processing is concerned, the possibility of obtaining position accuracies below 10^6 meters has been validated. Nevertheless, the true limitation of pulsar-based navigation has been found to be the required instrumentation. Very few radio pulsars can achieve a sufficiently high SNR with a small antenna to have reasonable integration times (few minutes) under the best possible conditions. Results have been obtained for a 10 m² antenna, assuming perfect cancellation of radio-frequency noise from the Sun and/or nearby planets, a constant speed model during the integration time, perfect antenna pointing (attitude control) and simultaneous pulsar observations. The technological effort does not only apply to the antenna but also to the signal bandwidth. It has been shown that increasing the bandwidth of the receiver leads to better accuracy. A technological limit of 200 MHz bandwidth at a central frequency of 1 GHz has been considered. Thus, front-end digital signal processing is also performing at high speed, with power consumption a critical factor.

A relaxation of the technological constraints considered in this study (smaller antennas, sequential rather than simultaneous observation of different pulsars, smaller receiver bandwidths, consideration of implementation loss and safety margins) is possible at the expense of much longer integration times. A reduction in the antenna area by a factor r must be compensated for with an increase in the integration time-bandwidth product of $1/r^2$. An integration time of many hours would be required to extract the faintest but more precise millisecond pulsars from noise. It is believed that for reduced-size antennas, the constant speed model will fail due to the necessity of estimating higher order derivatives of position. The highest technological impact is the issue between simultaneous or sequential observation of pulsars. The former requires as many antennas as observed pulsars but provides the fastest evolution of positioning accuracy versus time. The latter would further increase latency, the minimum time before a position estimate is produced (probably by a factor equal to the minimum number of required pulsars), as well as the ambiguity resolution algorithm. The smoothness of the spacecraft trajectory is believed to be more critical in the case of sequential observation.

The study of X-ray pulsars predicts longer integration times as arrival rates in the order of only 90 photons per hour have been reported for the usable X-ray pulsars, thus yielding over one day of integration (taking the ROSAT detector as a baseline). The number of available X-ray pulsars has been found to be much lower than for radio pulsars. Other pulsars with much higher flux densities as the Crab pulsar would drastically reduce the required integration times, but glitch-resilient signal processing should have to be devised and evaluated.

Summary: the authors of this study believe that the complexity involved for autonomous positioning at the spacecraft is rather involved.

| Pulsar | SNR (dB) | Q (dB) | T_o (min.) | σ_x (m.) | T_{50} (ms.) |
|----------|----------|----------|--------------|-----------------|----------------|
| B1937+21 | -55.6 | 8.90 | 40.13 | 5860 | 0.1 |
| B0736-40 | -50.2 | -10.72 | 4.02 | 1699492 | 29 |
| B1451-68 | -50.0 | -5.80 | 2.25 | 732540 | 12.5 |
| B0950+08 | -48.9 | -3.00 | 1.07 | 556730 | 9.5 |
| B0329+54 | -45.2 | 5.32 | 1.19 | 77681 | 6.6 |

Table 1: Minimum Integration times for the best pulsars, using an effective antenna area $A_e = 10\text{m}^2$ and the Gaussian pulse shape model. At least 100 pulsar periods have been considered in all cases. The quality factor Q is a measure of the relative goodness of each pulsar for timing estimation and T_{50} the pulse duration at half power.

Although pulsar positioning has been shown to be theoretically possible, issues of complexity and latency in obtaining position estimates cannot be met for *small* spacecraft capable of *fast* autonomous positioning. Rather, such a positioning system appears more suitable for large spacecraft or for hub stations providing telecommunication and location services to smaller spacecraft.

4 Vision

The technological requirements of pulsar navigation have been shown to be demanding. On one side, radio pulsars require large antennas while X-ray detectors, although much less bulky, have a limited life depending on their gas supply (apart from the faintness of usable X-ray pulsars). Although pulsars are extremely stable, effects such as glitches or pulsar proper motion somehow corrupt the 'neatness' of this timing reference if long-term missions are envisaged. The vision of the authors of this study is more toward a carefully engineered and controlled set of timing references, which, other than using naturally available sources, are tailored to the navigation problem. From our study of radio- and X-ray pulsars, we propose the following approaches:

4.1 Laser-based Navigation

It seems that the bulkiness of the antenna system, due to the extremely weak pulsar signal, would not be required if a network of laser signals were used to transmit carefully designed positioning information over the solar system (a solar-system-scale GPS). New generations of compact and efficient single-photon detectors combined with signal processing could be used on board spacecraft (note that in contrast to X-ray detectors, no gas supply is needed). The positioning algorithms would be more complex as the angular position of navigation beacons with respect to spacecraft would not be constant over the Solar System (which is the usual case) and it would be definitively more expensive in order to maintain this positioning network. For this approach to be justifiable, a suite of applications where autonomous navigation is necessary would be required. Note that the use of lasers for satellite and interplanetary communications is already under serious consideration.

4.2 Swarm navigation

Distributed signal detection and processing could be carried out by a satellite swarm. Depending on the swarm size, signals picked up by each swarm element could be combined to increase the quality with which pulsar (or maybe artificial beacon) signals are received. In the radio pulsar scenario, the difficulty associated with large antennas might be circumvented as a virtual set of distributed antennas with the same aggregate area could be implemented. In fact, a swarm should be considered a distributed array of detection and computation elements. The problem would be here on how to communicate and perform signal acquisition and navigation calculations over the satellite swarm: the swarm configuration may have to be estimated (we cannot predict the

complexity of this operation), as well as a common virtual clock. It would be important to determine what type of information should be exchanged between different members of the swarm to minimize the cost of inter-element communication. Collaborative schemes between elements of the swarm for performing communication (transmission/reception) operations with Earth appears to be also an interesting area of study, as important as navigation itself.

References

- [1] Andrew G. Lyne, Francis Graham-Smith, "Pulsar Astronomy", Cambridge University Press, 1998, ISBN 0 521 59413 8.
- [2] PSRCAT 2004, ATNF Pulsar Catalogue, <http://www.atnf.csiro.au/research/pulsar>
- [3] Hobbs, G., Faulkner, A., Stairs, I.H. et al, MNRAS (in press), 2004.
- [4] White, N.E. et al., in X-Ray Binaries, Cambridge Astrophysics Series, p.1, 1995.
- [5] Becker, W. and Trumper, J., A&A, 326, 682. 1997.
- [6] J.Sala et al. "Feasibility Study of a Spacecraft Navigation System Relying on Pulsar Timing Information", Technical University of Catalonia final report for ARIADNA project 03/4202, June 28th, 2004, European Space Agency Advanced Concepts Team, ESA/ESTEC, The Netherlands, <http://www.esa.int>
- [7] Gardner, W., "Introduction to Random Processes, with Applications to Signals and Systems", 2nd Edition. McGraw-Hill. 1990.
- [8] Kay, Steven M., "Fundamentals of Statistical Signal Processing - Estimation Theory", Prentice Hall Signal Processing Series, 1993, ISBN 0-13-345711-7.